A Load-Independent LCC-Compensated Wireless Power Transfer System for Multiple Loads With a Compact Coupler Design

Chenwen Cheng, Fei Lu, *Member, IEEE*, Zhe Zhou, Weiguo Li, Zhanfeng Deng, Fangyi Li, and Chris Mi, *Fellow, IEEE*

***Abstract*—This article proposes a novel wireless power transfer (WPT) system for multiple loads. Multiple coils are used as power repeaters to enhance the power transfer capability over a long distance and each power repeater corresponds to a load. The inductor-capacitor-capacitor (LCC) compensation method is used for each repeater coil in the system, which ensures load-independent currents flowing through the loads. Thus, flexible power control can be achieved for all the loads without affecting each other. In order to save space, the compensation coil is integrated with the repeater coil to realize a compact design. Bipolar coils are used for both the repeater coil and compensation coil. The undesirable coupling coefficient between the repeater coil and its compensation coil can be eliminated by putting them perpendicularly. The compensation coil is not only used to achieve resonant condition for the system, but also transfers energy to the next repeater coil via the magnetic coupling between them. The operational principle has been explained in detail. An experiment platform with six loads has been built and the experimental results are provided to validate the effectiveness of the proposed WPT repeater system. The maximum efficiency can reach 86.6%.**

***Index Terms*—Bipolar coil, compact coupler design, inductor-capacitor-capacitor (LCC) compensation, load-independent output currents, multiple loads, wireless power transfer (WPT).**

I. Introduction

WIRELESS power transfer (WPT) technology has been developing fast in recent years, which provides a new energy transfer method via the magnetic field [1]. In the conventional WPT system, only one load gets power from the source. However, the WPT system with multiple loads is interesting and deserves to be studied, as it can be used in some applications where the simultaneous charging of many electronic devices at different locations is possible.

In [2], a WPT system with two concentric receiving coils was designed. The two receiving coils are decoupled by alternating the winding direction of turns in one of the coils. A multi-load WPT system with different resonant frequencies for the receiving coils was designed in [3]. By setting the operational frequency of the transmitting coil equal to the resonant frequency of a receiving coil, the load connected to this receiving coil will obtain power. However, only one load can receive power at a specific frequency. A WPT system with multiple receivers was proposed in [4] for the battery cell voltage equalization. The printed circuit board technology is adopted to make the receiving coils in the same plane, which collect power simultaneously from a big transmitting coil. In this system, the coupling coefficients between any two receiving coils are assumed zero.

An alternative structure to transfer power wirelessly to multiple loads simultaneously is to use the repeater coils, which has been adopted in [5]–[7] to increase the power transfer distance. However, only one load is connected to the last coil, whereas the intermediate coils do not power any loads. In [8], the load is connected to each repeater coil so that the power can be transferred to these loads simultaneously. However, the load power is coupled with each other in such a topology, which means that when one load power changes, the power received in other coils will vary greatly. Thus, a load-independent WPT system needs to be studied to facilitate the power control.

Usually, compensation circuits with capacitors and inductors are used to improve the WPT system's performance, which can be classified as series–series (SS) [9], series–parallel [10], parallel–series [11], parallel–parallel [12], inductor-capacitor-capacitor (LCC)–LCC [13], etc. It is reported in [13] that the output current of the LCC–LCC compensated WPT system is constant when neglecting the coil parasitic resistances. Moreover, the amplitude of the load current is proportional to the coupling coefficient [13], which is different from the SS compensation topology where the amplitude of the load current is reversely proportional to the coupling coefficient [14]. Thus,

Manuscript received January 28, 2019; revised May 9, 2019; accepted July 3, 2019. Date of publication July 31, 2019; date of current version February 10, 2020. This work was supported by the Global Energy Interconnection Research Institute Company Ltd., (GEIRI) under Grant GEIRI-DL-71-17-011 (State Grid Sci & Tech Project: Research on the Magnetic-Resonant Wireless Power Transfer Technology for the High-Voltage Converter Valve in FACTS). *(Corresponding Author: Chris Mi.)*

C. Cheng and C. Mi are with San Diego State University, San Diego, CA 92182 USA (e-mail: cheng.cwen@gmail.com; mi@ieee.org).

F. Lu is with the Department of Electrical and Computer Engineering, Drexel University, Philadelphia, PA 19104 USA (e-mail: fei.lu@drexel.edu).

Z. Zhou, W. Li, Z. Deng, and F. Li are with the State Key Laboratory of Advanced Power Transmission Technology (Global Energy Interconnection Research Institute), Changping District, Beijing 102211, China (e-mail: zhouzhe@geiri.sgcc.com.cn; lwgmb90549@sina.com; iphone21@sina.com; 18811376167@163.com).

Color versions of one or more of the figures in this article are available online at http://ieeexplore.ieee.org.

Digital Object Identifier 10.1109/TIE.2019.2931260

the WPT system with the LCC compensation topology is much safer because the high load current can be avoided when there is a misalignment between the coils.

A novel multiload WPT system using repeater coils is proposed in this article and the LCC compensation is adopted for all the repeater coils. In each LCC compensation circuit, there are two compensation capacitors and one compensation inductor. Usually the compensation inductor occupies more space, which increases the system's volume. In order to save space for the LCC-compensated WPT system, different coupler pads with compact coil design methods have been proposed [15]–[18]. In [18], bipolar coils are adopted for the compensation inductors, which are placed perpendicularly to each other to eliminate the coupling effect between the two compensation coils. Unipolar coils are used for the main coils so that the coupling effects between the compensation coils and the main coils can also be eliminated. In this article, the bipolar coils are adopted in the proposed WPT repeater system for not only the compensation coils but also for the repeater coils. The repeater coil and its corresponding compensation coil are placed perpendicularly so that the coupling effect between them can be eliminated. As a result, the repeater coil and its compensation coil can be placed coaxially to achieve a compact design. One of the innovations in this article is that the compensation coil is not only used to achieve the resonating state for the system, but also coupled with its next repeater coil. Thus, energy can be transferred from the compensation coil to its next repeater coil.

Such a design can be proved to have the load-independent load current characteristics, as will be shown in Section II, which is the most significant contribution of this article. The proposed WPT system can be used to power the gate drivers of the power electronics switches in a multi-level converter [19]. In such an application, the reference potentials of these switches are different from each other, an isolated power supply should be used for each gate driver. Because no direct contact is needed in the proposed WPT system, high insulation level can be ensured. An experimental setup with six loads has been built to validate the effectiveness of the proposed topology.

II. System Description

A. System Structure

The structure of the proposed WPT system using LCC compensation topology is shown in Fig. 1. There are $(N+1)$ LCC units in the system, i.e., LCC #0–#N, each of which consists of a repeater coil L_n, a compensation coil L_{fn}, and two compensation capacitors C_n and C_{fn} $(n = 0, 1, 2, \ldots, N)$. LCC #0 is connected to the inverter and functions as the transmitter. LCC #n $(n = 1, 2, \ldots, N)$ receives power from its previous LCC circuit via magnetic coupling between $L_{f(n-1)}$ and L_n, and transfers power to both the local load and the subsequent LCC circuit via magnetic coupling between L_{fn} and L_{n+1}. Thus, L_n and L_{fn} can be regarded the receiving and transmitting coils, respectively. Usually the load circuit should contain a rectifier to transform the ac power to a dc source for the load. Considering that the current flowing through and the voltage across the rectifier are in phase, the load can be regarded as resistive [13]. Thus, the real load is modeled as load resistors R_n $(n = 1, 2, \ldots, N)$ for simplification, which is connected in series with the corresponding compensation coil L_{fn}.

In the proposed WPT system, only the magnetic coupling between $L_{f(n-1)}$ and L_n $(n = 1, 2, \ldots, N)$ is considered while the coupling between other coils is too small so that they can be omitted with the coil design method proposed in Section III. It can be seen that $L_{f(n-1)}$ $(n = 1, 2, \ldots, N)$ not only functions as the compensation inductance, but also transfers power to the next LCC circuit via the magnetic field. The mutual inductance and coupling coefficient between $L_{f(n-1)}$ and L_n is defined as M_n and k_n, respectively, which have the relationship

$$k_n = M_n / \sqrt{L_{f(n-1)} \cdot L_n}, \quad n = 1, 2, \ldots, N. \tag{1}$$

B. Working Principle Analysis

The fundamental harmonics approximation (FHA) method is used to analyze the system. Then, the circuit model of the proposed WPT system using the LCC compensation method can be obtained, as shown in Fig. 2(a). ω_0 is the operational angular frequency of the system. $\boldsymbol{V}_0$ is the output voltage of the inverter. $\boldsymbol{I}_n$ and $\boldsymbol{I}_{fn}$ $(n = 0, 1, 2, \ldots, N)$ are the currents flowing through L_n and L_{fn}, respectively, the directions of which are positive when the currents flow into the dot terminals of these coils. The voltages across the load resistances are noted as $\boldsymbol{V}_1, \boldsymbol{V}_2, \ldots, \boldsymbol{V}_n$, respectively.

In the LCC-compensated WPT system, the inductances and capacitances should meet the following equation to achieve a resonant condition [13]:

$$1/\omega_0^2 = L_{fn} \cdot C_{fn} = (L_n - L_{fn}) \cdot C_n, \quad n = 0, 1, 2, \ldots, N. \tag{2}$$

When neglecting the magnetic saturation of the inductances and the nonlinearity of the inverter, the system can be regarded as a linear circuit. Thus, the superposition theory can be used to analyze the operational principle of the proposed WPT system. The load resistance can be replaced with a voltage source whose value equals the voltage across the resistance $(\boldsymbol{V}_n, n = 1, 2, \ldots, N)$. Then, the effects of the input voltage $\boldsymbol{V}_0$ and the load voltages $\boldsymbol{V}_n$ can be analyzed separately, as shown in Fig. 2(b) and (c).

In Fig. 2(b), only the input voltage $\boldsymbol{V}_0$ is considered while all the load voltages $\boldsymbol{V}_n$ are shorted. The additional suffix "a" in the currents such as $\boldsymbol{I}_{f0,a}$ and $\boldsymbol{I}_{0,a}$ indicates that these currents are generated by $\boldsymbol{V}_0$. First, the last unit LCC #N is considered. Since L_{fN} resonates with C_{fN} according to (2), the impedance of the parallel circuit of L_{fN} and C_{fN} is infinite, which results in an open circuit for C_N. Thus, the current flowing through L_N and C_N, i.e., $\boldsymbol{I}_{N,a}$ is zero. Then, the induced voltage in coil $L_{f(N-1)}$ generated by $\boldsymbol{I}_{N,a}$, i.e., $j\omega_0 M_N \boldsymbol{I}_{N,a}$, is also zero. Similar to LCC #N, $L_{f(N-1)}$ resonates with $C_{f(N-1)}$ and another open circuit forms for C_{N-1}. Thus, the current flowing through L_{N-1} is zero. The analysis process can be implemented one by one iteratively starting from the last unit to the first one. For the LCC unit #n, it can be found that L_{fn} resonate with C_{fn}, and an open circuit forms for C_n. Thus, $\boldsymbol{I}_{n,a}$ is zero where

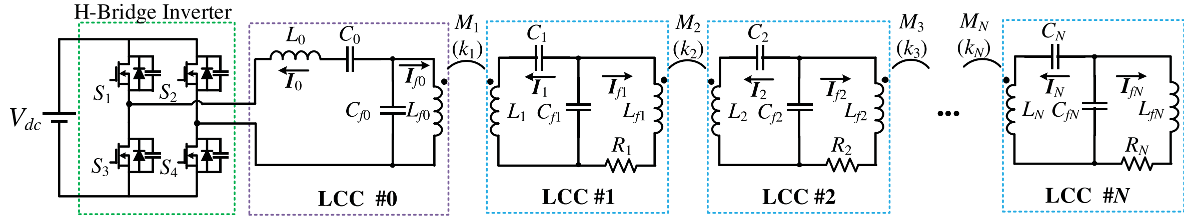

Fig. 1. Structure of the proposed WPT system using LCC compensation.

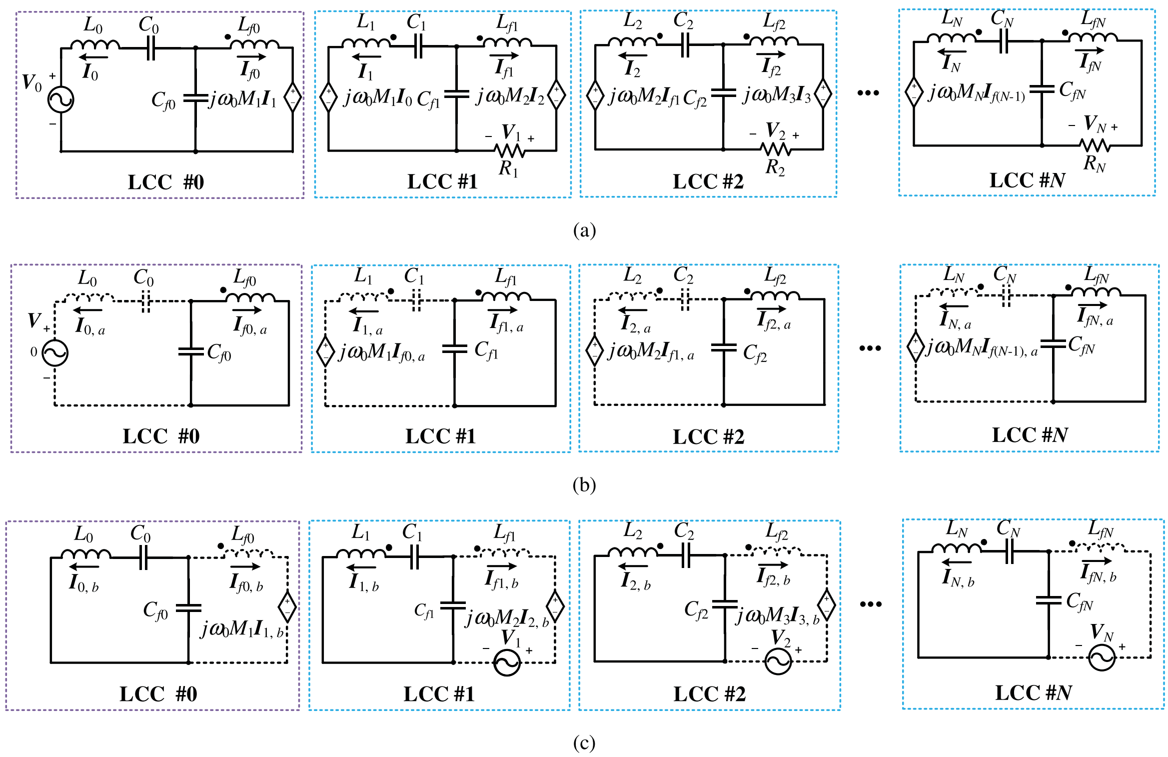

Fig. 2. Circuit analysis of the proposed WPT system using FHA method. (a) Equivalent circuit model using FHA method. (b) When only $\boldsymbol{V}_0$ is applied. (c) When only the other voltage sources are applied.

n ranges from 0 to N, i.e.,

$$\boldsymbol{I}_{n,a} = 0, \quad n = 0, 1, 2, \ldots, N. \tag{3}$$

As a result, the induced voltages caused by $\boldsymbol{I}_{n,\,a}$ in the compensation coils $L_{f(n-1)}$ is zero as well.

Then, the currents flowing through the compensation coils L_{fn} ($n = 0, 1, 2, \ldots, N$) are equal to the currents flowing through the respective compensation capacitance C_{fn} ($n = 0$, $1, 2, \ldots, N$), which can be calculated as

$$\begin{cases} \boldsymbol{I}_{f0,a} = \boldsymbol{V}_0 / j\omega_0 L_{f0} \\ \boldsymbol{I}_{fn,a} = M_n \boldsymbol{I}_{f(n-1),a} / L_{fn}, \quad n = 1, 2, 3, \ldots, N \end{cases}. \tag{4}$$

Fig. 2(c) shows the circuit model when only the load voltage sources $\boldsymbol{V}_n$ ($n = 1, 2, \ldots, N$) are applied. The additional suffix "b" in the currents such as $\boldsymbol{I}_{f0,\,b}$ and $\boldsymbol{I}_{0,\,b}$ indicates that these currents are generated by the load voltage sources $\boldsymbol{V}_n$ ($n = 1, 2, \ldots, N$). The input voltage source $\boldsymbol{V}_0$ is shorted. Then, L_n, C_n, and C_{fn} form a parallel resonant circuit, which can be treated as an open circuit. Thus, the current flowing through L_{fn} equals zero, i.e.,

$$\boldsymbol{I}_{fn,b} = 0, \quad n = 0, 1, 2, \ldots, N. \tag{5}$$

Then, the induced voltage $j\omega_0 M_n \boldsymbol{I}_{f(n-1),\,b}$ in L_n is zero. In order to calculate the currents flowing through the repeater coils, LCC #N can be considered first. Then, the currents flowing through the repeater coils in the other units can be deduced iteratively, which is summarized as

$$\begin{cases} \boldsymbol{I}_{N,b} = \boldsymbol{V}_N / j\omega_0 L_{fN} \\ \boldsymbol{I}_{n,b} = \mathbf{V}_n / j\omega_0 L_{fn} \\ \qquad + M_{n+1} \mathbf{I}_{n+1,b} / L_{fn}, \quad n = 0, 1, 2, \ldots, N-1 \end{cases}. \tag{6}$$

The real currents flowing through the coils in the system are the sum of the currents when considering $\boldsymbol{V}_0$ and the other load voltages $\boldsymbol{V}_n$ ($n = 1, 2, \ldots, N$), respectively, which can be calculated as follows by taking (3)–(6) into account:

$$\begin{cases} \boldsymbol{I}_{f0} = \boldsymbol{I}_{f0,a} + \boldsymbol{I}_{f0,b} = \boldsymbol{V}_0/j\omega_0 L_{f0} & \\ \boldsymbol{I}_{fn} = \boldsymbol{I}_{fn,a} + \boldsymbol{I}_{fn,b} & \\ \quad = M_n \boldsymbol{I}_{f(n-1)}/L_{fn}, & n = 1, 2, \ldots, N \\ \boldsymbol{I}_N = \boldsymbol{I}_{N,a} + \boldsymbol{I}_{N,b} = \boldsymbol{V}_N/j\omega_0 L_{fN} & \\ \boldsymbol{I}_n = \boldsymbol{I}_{n,a} + \boldsymbol{I}_{n,b} = \boldsymbol{V}_n/j\omega_0 L_{fn} & \\ \quad + M_{n+1}\boldsymbol{I}_{n+1}/L_{fn}, & n = 0, 1, \ldots, N-1 \end{cases} \tag{7}$$

As can be seen from (7), all the currents flowing through the compensation coils $\boldsymbol{I}_{fn}$ ($n = 0, 1, 2, \ldots, N$) are in phase, which lags $\boldsymbol{V}_0$ by 90°. Because the loads are considered resistive, $\boldsymbol{V}_n$ is also in phase with $\boldsymbol{I}_{fn}$ ($n = 1, 2, \ldots, N$). The current in the repeater coils $\boldsymbol{I}_n$ lags $\boldsymbol{I}_{fn}$ by 90° based on (7). Because $\boldsymbol{I}_0$ and $\boldsymbol{V}_0$ are opposite in phase, the unit power factor can be achieved for the inverter.

C. Load-Independent Load Currents

As can be seen from (7), the load currents that flow through the compensation coil L_{fn} in the repeater units are only related to the input voltage $\boldsymbol{V}_0$, the angular frequency ω_0, the mutual inductances between adjacent units M_n, and the compensation inductances L_{fn}. The load resistances will not affect the magnitudes of the load currents if neglecting the parasitic resistances. Thus, the load-independent load current characteristics are obtained, which is especially suitable for practical applications with variable loads. When one load changes, it will not affect the currents in other loads so that the load power can be adjusted flexibly without the need of introducing complicated control strategies.

Moreover, the amplitudes of all the load currents are identical if the following equation is met:

$$M_1 = M_2 = \cdots = M_N = L_{f1} = L_{f2} = \cdots = L_{fN} = M. \tag{8}$$

III. Coil Design

As discussed above, in order to obtain constant load current characteristics, only the magnetic coupling between L_{fn} and $L_{(n+1)}$ ($n = 0, 1, 2, \ldots, N-1$) is needed while the coupling between other coils, even the repeater coil and the compensation coil in the same LCC unit, should be designed as small as possible so that it can be omitted. A specific coil topology method is provided in this section.

In the system, the bipolar coil is used for both the repeater coil and the compensation coil, as shown in Fig. 3. Both the repeater coil and the compensation coil are square with the side length of l_L and l_{Lf}, respectively. In a LCC compensated WPT system, the self-inductance of the compensation inductor should be smaller than that of the main coil [13]. Usually the compensation coil is small in volume. In order to increase the magnetic coupling between L_{fn} and $L_{(n+1)}$ ($n = 0, 1, 2, \ldots, N-1$), the compensation coil in the proposed system is designed with the same side length but a smaller coil width, i.e., $l_L = l_{Lf}$ and $l_{w\_L} > l_{w\_Lf}$.

The whole system structure modeled using MAXWELL is shown in Fig. 4. In LCC #n, L_n, Fe_n, and L_{fn} form a sandwich

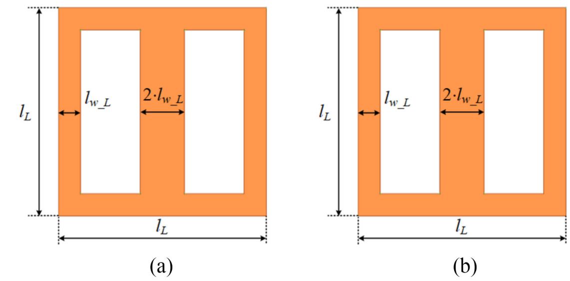

Fig. 3. (a) and (b) Repeater and compensation coils, respectively, used in the proposed WPT system.

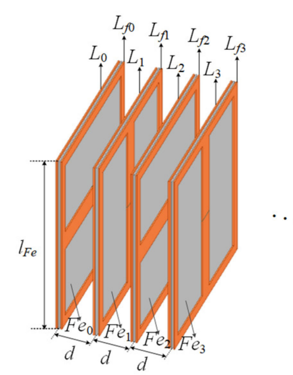

Fig. 4. Simulation model of the proposed WPT system.

structure, where L_n and L_{fn} are fixed on the two sides of the ferrite plate Fe$_n$, respectively. The repeater coil L_n is placed coaxially with its compensation coil L_{fn} so that a compact structure can be obtained. Moreover, they are placed perpendicularly, so that the coupling effect between them can be neglected [18]. A ferrite plate (Fe$_n$) is inserted between L_n and L_{fn} ($n = 0, 1, 2, \ldots, N$) with a side length of l_{Fe}. The ferrite plates can not only increase the magnetic coupling between adjacent LCC units, but also suppress the magnetic coupling between non-adjacent coils such as between L_0 and L_{f1}.

In the designed example of the WPT system, the distance between two adjacent LCC units is set as $d = 30$ mm. The side length of the coil is designed as $l_L = l_{Lf} = 150$ mm. Because of the system's symmetrical characteristics, two adjacent LCC units, such as LCC #0 and LCC #1, are enough to analyze the system. k_1 is the coupling coefficient between L_{f0} and L_1. The ratio between l_{w_Lf} and l_{w_L} is defined as $r_w = l_{w\_Lf}/l_{w\_L}$. As can be seen from Fig. 5, k_1 increases gradually as l_{w_L} increases from 10 to 20 mm when r_w is fixed. The increasing rate of k_1 slows down when l_{w_L} is larger than 16 mm. Moreover, a larger k_1 comes with a larger r_w. However, the influence of r_w on k_1 is smaller than l_{w_L}. Based on the simulation results shown in Fig. 5, l_{w_L} is chosen to be 16 mm and r_w is set as 0.5, which means l_{w_Lf} is 8 mm. Thus, a high coupling coefficient k_1 can be obtained.

In order to study the influence of the ferrite plate length l_{Fe} on the coupling coefficient, Fig. 6 shows the coupling coefficient variations as l_{Fe} increases, where k_{0_f0}, k_{0_1}, and k_{0_f1} are the coupling coefficients between L_0 and L_{f0}, L_0 and L_1, and L_0 and L_{f1}, respectively. k_{0_f0} and k_{0_1} remains very small as l_{Fe} varies

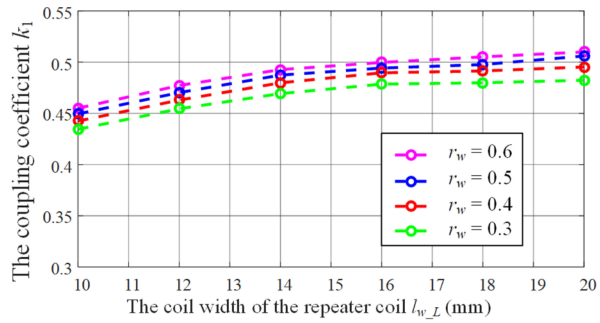

Fig. 5. Variations of k_1 with different coil widths l_{w_L} and coil width ratios r_w between l_{w_Lf} and l_{w_L}.

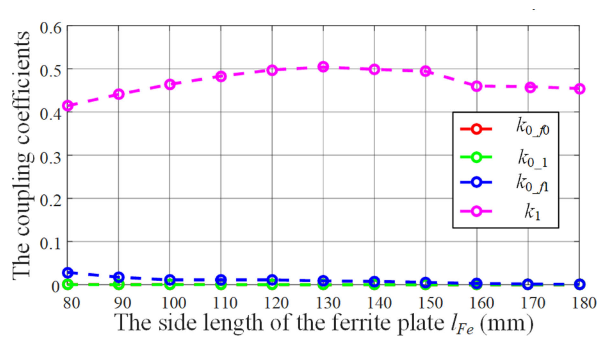

Fig. 6. Coupling coefficient variations versus the length of the ferrite l_{Fe}.

because L_0 is placed perpendicularly with L_{f0} or L_1. k_{0_f1} keeps decreasing as l_{Fe} increases, which means a larger ferrite plate is beneficial for enhancing the magnetic decoupling between non-adjacent coils. k_1 increases first and then decreases. When l_{Fe} is between 110 and 150 mm, k_1 can maintain a high value. To minimize the influence of the undesired coupling coefficient k_{0_f1}, l_{Fe} can be selected as 150 mm and k_1 is about 0.48.

IV. Power Transfer Capability Analysis

In Section II, the load characteristics of the proposed LCC compensated multiload system is analyzed using the superposition theory. It is verified that the amplitudes of the load currents are constant and regardless of the loads when neglecting the coils' parasitic resistances. In practical applications, the parasitic resistances are inevitable, the influence of which on the load currents will be analyzed here.

The reflected impedance is used to facilitate the analysis process, which is the equivalent impedance of all the subsequent coils in a designated coil. For the compensation coil L_{fN} in LCC #*N*, the reflection impedance Z_{fN} is equal to 0 because there is no other coil after L_{fN}. Then, the impedance in each coil can be calculated one by one from the last coil as

$$\begin{cases} Z_{fN} = 0 \\ Z_n = (\omega_0 L_{fn})^2/(r_{fn} + R_n + Z_{fn}), \quad n = 0, 1, 2, \ldots, N \\ Z_{fn} = (\omega_0 M_{f(n+1)})^2/(r_{n+1} + Z_{n+1}), \quad n = 0, 1, 2, \ldots, N-1 \end{cases} \tag{9}$$

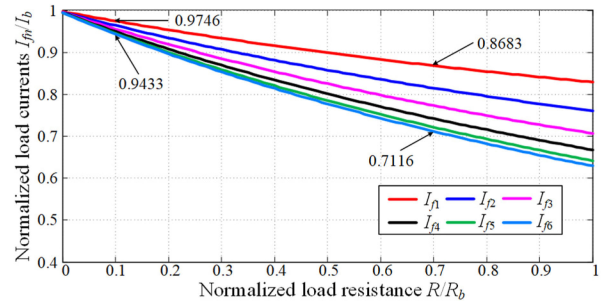

Fig. 7. Load current variations against the increasing load resistance ($k = 0.5$, $Q = 200$, and $Q_f = 100$).

where Z_n and Z_{fn} are the reflection impedances in coil L_n and L_{fn}, respectively; and r_n and r_{fn} are the parasitic resistances of L_n and L_{fn}, respectively. If the quality factors of L_n and L_{fn} are defined as Q_n and Q_{fn}, respectively, r_n and r_{fn} can be calculated as

$$r_n = \omega_0 L_n/Q_n, r_{fn} = \omega_0 L_{fn}/Q_{fn}, \quad n = 0, 1, 2, \ \ldots, N. \tag{10}$$

Based on the coil design method proposed in Section III, all the repeaters are identical, so are the compensation coils, i.e.,

$$\begin{aligned} Q_1 &= Q_2 = \cdots = Q_N = Q, \\ Q_{f1} &= Q_{f2} = \cdots = Q_{fN} = Q_f. \end{aligned} \tag{11}$$

The coupling coefficients between adjacent units are also identical, i.e.,

$$k_1 = k_2 = \cdots = k_N = k. \tag{12}$$

Then, the currents flowing through each coil can be calculated iteratively using the reflection impedance defined in (9) as

$$\begin{cases} \boldsymbol{I}_0 = -\boldsymbol{V}_0/(r_0 + Z_0) \\ \boldsymbol{I}_{fn} = j\omega_0 L_{fn} \boldsymbol{I}_n/(r_{fn} + R_n + Z_{fn}), \quad n = 0, 1, 2, \ldots, N. \\ \boldsymbol{I}_n = -j\omega_0 M_n \boldsymbol{I}_{f(n-1)}(r_n + Z_n), \quad n = 1, 2, 3, \ldots, N \end{cases} \tag{13}$$

Based on (8)–(13), the load currents are obtained when the load resistances vary, as shown in Fig. 7, where $k = 0.5$, $Q = 200$, and $Q_f = 100$. It is assumed that all the load resistances are identical to facilitate the analysis, i.e.,

$$R_1 = R_2 = \cdots = R_N = R. \tag{14}$$

It needs to be clarified that although in the analysis the load resistances are the same, it does not mean in real applications all the loads should be identical at any time. The proposed WPT system can also work normally with different load resistances as validated in Section V.

In order to facilitate comparisons, the load resistances and currents are normalized by dividing their base values defined as follows:

$$R_b = \omega_0 M, \quad I_b = V_0/R_b. \tag{15}$$

It can be seen from Fig. 7 that the load currents decrease gradually as the load resistance *R* increases. The farther the distance

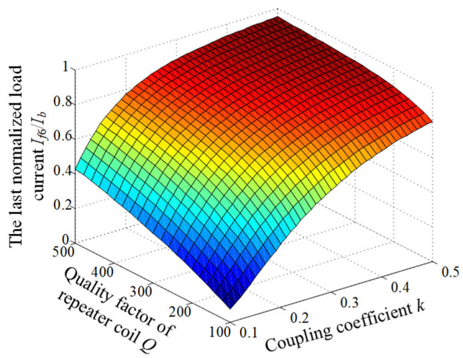

(a)

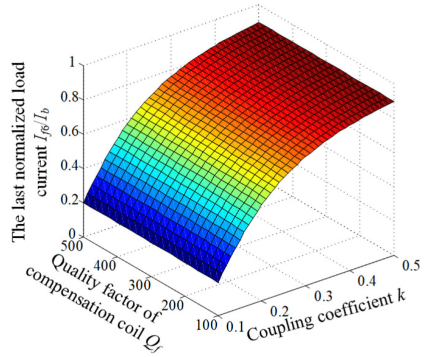

(b)

Fig. 8. Last load current variation against (a) coupling coefficient k and the quality factor of the repeater coil Q ($R/R_b = 0.2$ and $Q_f = 100$) and (b) coupling coefficient k and the quality factor of the compensation coil Q_f ($R/R_b = 0.2$, $Q = 200$).

between the load and LCC #0, the faster the load current drops. For example, when the normalized load resistance increases from 0.1 to 0.7, the normalized load current I_{f1} decreases from 0.9746 to 0.8683, whereas I_{f6} decreases from 0.9433 to 0.7116. Thus, the last load current can be regarded as the criterion for judging the constant load current characteristics. If the last load current drops less when R increases, the system will have better constant load current characteristics.

Fig. 8 shows the variation of the last load current I_{f6} versus the variations of the coupling coefficient k, the quality factor Q of the repeater coil and the quality factor Q_f of the compensation coil when $N = 6$ and $R/R_b = 0.2$. It can be seen that a larger k, Q, or Q_f leads to a smaller drop of I_{f6}, which means better constant current characteristics can be obtained. Comparing Fig. 8(a) and (b), the quality factor Q of the repeater coil has a larger influence on the load current than the quality factor Q_f of the compensation coil.

V. Experimental Results

An experimental setup with six loads is constructed in this section, as shown in Fig. 9. An inverter consisting of four SiC MOSFETs is used to generate the high-frequency ac source for the system. The dimensions of the repeater coil, the compensation coil, and the ferrite plate are all 150 × 150 mm, which is consistent with the simulation settings discussed in Section III. The turns numbers of the repeater coil and compensation coil are 12 and 5, respectively. The detailed parameters of the experimental setup are listed in Table I.

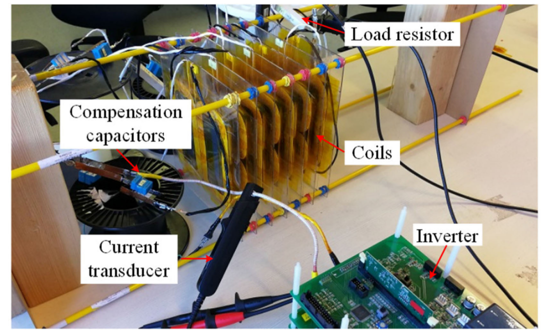

Fig. 9. System structure of the experimental setup.

TABLE I
Circuit Parameters of the Experimental Setup

Parameter	Value	Parameter	Value
V_{dc}	30V	f_s	200kHz
L_0~L_6	120μH	L_{f0}~L_{f6}	29.5μH
Q_0~Q_6	200	Q_{f0}~Q_{f6}	120
C_0 ~ C_6	6.96nF	C_{f0} ~ C_{f6}	21.84nF
k	0.49	d	30mm

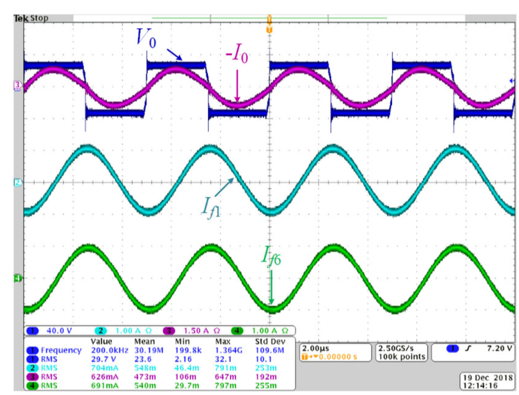

Fig. 10. Experimental load current waveforms.

Fig. 10 shows the experimental waveforms of the setup. The input voltage $\boldsymbol{V}_0$ and the input current $-\boldsymbol{I}_0$ are nearly in phase, which indicates that the power factor is almost 1. Since the oscilloscope has only four channels, only $\boldsymbol{I}_{f1}$ and $\boldsymbol{I}_{f6}$ are shown, which have almost the same amplitude and phase angle.

Fig. 11 shows the amplitude variations of the six load currents against the increasing load resistance where the six load resistances have the same value. Because of the coils' parasitic resistances, the load current decrease gradually, as discussed above. The measured load currents are basically consistent with the calculated results.

The system efficiency as a function of load resistance is illustrated in Fig. 12. The solid line is the calculated efficiency,

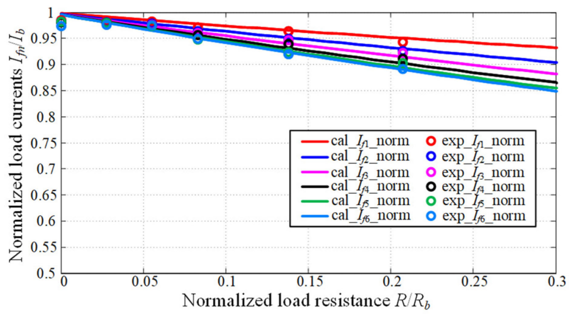

Fig. 11. Load current variations against the load resistance.

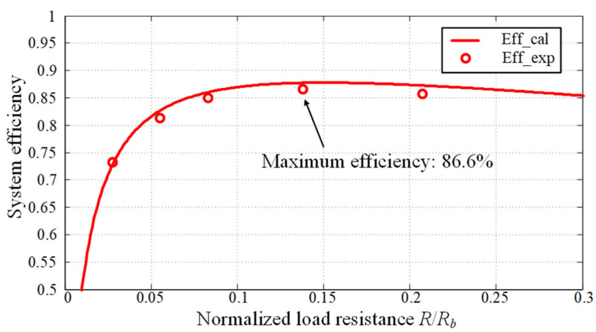

Fig. 12. System efficiency against the load resistance.

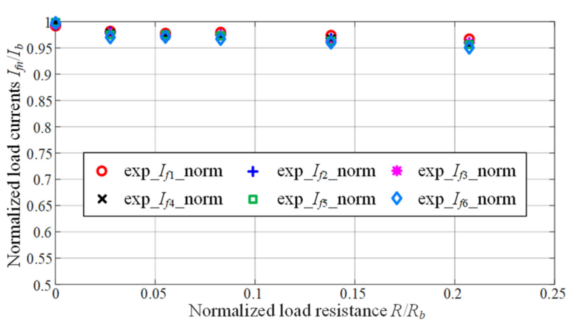

Fig. 13. Load currents' variations against the increasing load resistance ($R_2 = R_4 = R_6 = 0$; R_1, R_3, and R_5 have the same and varying load resistances).

whereas the dots represent the measured values. The efficiency can be calculated through dividing the total load power, which can be obtained by multiplying the square of the load current in (13) and the load resistance R, by the input power. When the normalized load resistance is about 0.14, the system efficiency can reach its maximum value of 86.6%. Considering that there are totally six loads in the system, the efficiency is quite high. If the coupling coefficient or the coil's quality factor is larger, the system efficiency can be enlarged further.

Fig. 13 shows the variations of the load current with the increasing load resistances, where $R_2 = R_4 = R_6 = 0$ and R_1, R_3, and R_5 have identical and varying load resistances. It can be seen that, in this condition, the variation of the load current is within 5%, which is small and acceptable.

Fig. 14 shows the load current with six different load resistances. The red circle points shown in Fig. 14 represent the

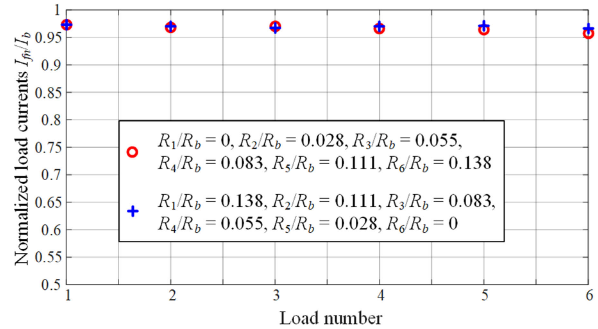

Fig. 14. Load currents' variations with different load resistances.

six load current, where $R_1/R_b = 0$, $R_2/R_b = 0.018$, $R_3/R_b = 0.055$, $R_4/R_b = 0.083$, $R_5/R_b = 0.111$, and $R_6/R_b = 0.138$, while the blue cross points represent the six load currents, where $R_1/R_b = 0.138$, $R_2/R_b = 0.111$, $R_3/R_b = 0.0830$, $R_4/R_b = 0.055$, $R_5/R_b = 0.018$, and $R_6/R_b = 0$. It can be seen that in both the cases, the load currents remain almost constant.

The experimental results show that the load current in the proposed WPT system is almost load independent in different load conditions.

VI. Conclusion

In this article, a novel WPT system using repeater coils for multiple loads was proposed. The repeater coils enabled the power transfer with a high efficiency, each of which was compensated with the LCC topology and corresponded to a load. The LCC compensation results in the load-independent currents were flowing through all the loads. Thus, the load power could be flexibly controlled without affecting each other, which was the most outstanding advantage of the proposed system. In order to save space, a compact coil design was proposed, where two bipolar coils were used for both the repeater coil and the compensation coil in the same LCC circuit. These two coils were placed perpendicularly with each other so that the coupling effect between them could be eliminated even when they were placed close to each other, which greatly decreased the system complexity. The compensation coil was not only used to achieve a resonant state for the system, but also to transfer energy to the next LCC circuit via magnetic coupling. The coil design technique was provided with the help of a three-dimensional finite-element analysis (FEA) simulation tool. An experiment setup with six loads was established and the experimental results validated the effectiveness of the proposed WPT system. The proposed WPT system can be used to power the multiple driver circuits in a multilevel converter.

References

[1] Z. Zhang, H. Pang, A. Georgiadi, and C. Cecati, "Wireless power transfer – An overview," *IEEE Trans. Ind. Electron.*, vol. 66, no. 2, pp. 1044–1058, Feb. 2019.

[2] U. Pratik, B. J. Varghese, A. Azad, and Z. Pantic, "Optimum design of decoupled concentric coils for operation in double—receiver wireless power transfer systems," *IEEE J. Emerg. Sel. Topics Power Electron.*, vol. 7, no. 3, pp. 1982–1998, Sep. 2019.

[3] Y. Zhang, T. Lu, Z. Zhao, F. He, K. Chen, and L. Yuan, "Selective wireless power transfer to multiple loads using receivers of different resonant frequencies," *IEEE Trans. Power Electron.*, vol. 30, no. 11, pp. 6001–6005, Nov. 2015.

[4] M. Liu, M. Fu, Y. Wang, and C. Ma, "Battery cell equalization via megahertz multiple-receiver wireless power transfer," *IEEE Trans. Power Electron.*, vol. 33, no. 5, pp. 4135–4144, May 2018.

[5] W. X. Zhong, C. K. Lee, and S. Y. R. Hui, "Wireless power domino-resonator systems with noncoaxial axes and circular structures," *IEEE Trans. Power Electron.*, vol. 27, no. 11, pp. 4750–4762, Nov. 2012.

[6] C. K. Lee, W. X. Zhong, and S. Y. R. Hui, "Effects of magnetic coupling of nonadjacent resonators on wireless power domino-resonator systems," *IEEE Trans. Power Electron.*, vol. 27, no. 4, pp. 1905–1916, Apr. 2012.

[7] D. Ahn and S. Hong, "A study on magnetic field repeater in wireless power transfer," *IEEE Trans. Ind. Electron.*, vol. 60, no. 1, pp. 360–371, Jan. 2013.

[8] Y. Zhang, T. Lu, Z. Zhao, K. Chen, F. He, and L. Yuan, "Wireless power transfer to multiple loads over various distances using relay resonators," *IEEE Microw. Wireless Compon. Lett.*, vol. 25, no. 5, pp. 337–339, May 2015.

[9] X. Qu, W. Zhang, S.-C. Wong, and C. K. Tse, "Design of a current-source-output inductive power transfer LED lighting system," *IEEE J. Emerg. Sel. Topics Power Electron.*, vol. 3, no. 1, pp. 306–314, Mar. 2015.

[10] J. L. Villa, J. Sallan, J. F. S. Osorio, and A. Llombart, "High-misalignment tolerant compensation topology for ICPT systems," *IEEE Trans. Ind. Electron.*, vol. 59, no. 2, pp. 945–951, Feb. 2012.

[11] J. Sallan, J. L. Villa, A. Llombart and J. F. Sanz, "Optimal design of ICPT systems applied to electric vehicle battery charge," *IEEE Trans. Ind. Electron.*, vol. 56, no. 6, pp. 2140–2149, Jun. 2009.

[12] C. S. Wang, G. A. Covic, and O. H. Stielau, "Power transfer capability and bifurcation phenomena of loosely coupled inductive power transfer systems," *IEEE Trans. Ind. Electron.*, vol. 51, no. 1, pp. 148–157, Feb. 2004.

[13] S. Li, W. Li, J. Deng, T. D. Nguyen, and C. C. Mi, "A double-sided LCC compensation network and its tuning method for wireless power transfer," *IEEE Trans. Veh. Technol.*, vol. 64, no. 6, pp. 2261–2273, Jun. 2015.

[14] W. Zhang, S. C. Wong, C. K. Tse, and Q. Chen, "Load-independent duality of current and voltage outputs of a series- or parallel-compensated inductive power transfer converter with optimized efficiency," *IEEE J. Emerg. Sel. Topics Power Electron.*, vol. 3, no. 1, pp. 137–146, Mar. 2015.

[15] J. Deng, W. Li, T. D. Nguyen, S. Li, and C. C. Mi, "Compact and efficient bipolar coupler for wireless power chargers: design and analysis," *IEEE Trans. Power Electron.*, vol. 30, no. 11, pp. 6130–6140, Nov. 2015.

[16] F. Lu, H. Zhang, H. Hofmann, W. Su, and C. C. Mi, "A dual-coupled LCC-compensated IPT system with a compact magnetic coupler," *IEEE Trans. Power Electron.*, vol. 33, no. 7, pp. 6391–6402, Jul. 2018.

[17] T. Kan, T.-D. Nguyen, J. C. White, R. K. Malhan, and C. C. Mi, "A new integration method for an electric vehicle wireless charging system using LCC compensation topology: Analysis and design," *IEEE Trans. Power Electron.*, vol. 32, no. 2, pp. 1638–1650, Feb. 2017.

[18] T. Kan, F. Lu, T.-D. Nguyen, P. P. Mercier, and C. C. Mi, "Integrated coil design for EV wireless charging systems using LCC compensation topology," *IEEE Trans. Power Electron.*, vol. 33, no. 11, pp. 9231–9241, Nov. 2018.

[19] M. Takasaki, Y. Miura, and T. Ise, "Wireless power transfer system for gate power supplies of modular multilevel converters," in *Proc. IEEE Int. Power Electron. Motion Control Conf. ECCE Asia*, May 2016, pp. 3183–3190.

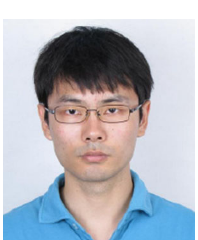

Chenwen Cheng received the B.S. and Ph.D. degrees in electrical engineering from Zhejiang University, Hangzhou, China, in 2012 and 2017, respectively.

He is currently a Postdoc Researcher with San Diego State University, San Diego, CA, USA. His research interests include motor control, renewable power generation, and wireless power transfer technologies.

Fei Lu (S'12–M'17) received the B.S. and M.S. degrees from the Harbin Institute of Technology, Harbin, China, in 2010 and 2012, respectively, and the Ph.D. degree from the University of Michigan, Ann Arbor, MI, USA, in 2017, all in electrical engineering.

He is currently an Assistant Professor with the Department of Electrical and Computer Engineering, Drexel University, Philadelphia, PA, USA. His research interest focuses on power electronics and the application of electric vehicle charging.

Zhe Zhou received the B.E. degree in measure and control technology and instrumentations from the Changchun University of Science and Technology, Changchun, China, in 2011, and the M.S. degree in power electronics and power drives from Tianjin University, Tianjin, China, in 2014.

He is currently with the State Key Laboratory of Advanced Power Transmission Technology (Global Energy Interconnection Research Institute), Changping District, Beijing, China. His research interests include applications of the wide-gap device and the power electronic transformer.

Weiguo Li received the B.S. degree from Northeast Dianli University, Jilin, China, in 1996, the M.S. degree from China Electric Power Research Institute, Beijing, China, in 2006, and the Ph.D. degree from North China Electric Power University, Beijing, China, in 2013, all in electrical engineering.

He is currently with the State Key Laboratory of Advanced Power Transmission Technology (Global Energy Interconnection Research Institute), Changping District, Beijing. His research interests include flexible ac transmission systems and power systems.

Zhanfeng Deng received the B.S. and M.S. degrees in welding technology and equipment from Jilin Polytechnical University, Changchun, China, in 1996, and the Ph.D. degree in electrical engineering from Tsinghua University, Beijing, China, in 2003.

He is currently with the State Key Laboratory of Advanced Power Transmission Technology (Global Energy Interconnection Research Institute), Changping District, Beijing. His research interests include flexible ac transmission systems and power systems.

Fangyi Li received the B.E. degree in thermal and dynamic engineering from the School of Energy, Power and Mechanical Engineering, North China Electric Power University, Beijing, China, in 2015, and the M.S. degree in electrical engineering from North China Electric Power University, Beijing, in 2018.

He is currently with the State Key Laboratory of Advanced Power Transmission Technology (Global Energy Interconnection Research Institute), Changping District, Beijing. His research interests include electromagnetic compatibility of power electronic devices and application of controllable lightning arrester.

Chris Mi (S'00–A'01–M'01–SM'03–F'12) received the B.S.E.E. and M.S.E.E. degrees from Northwestern Polytechnical University, Xi'an, China, and the Ph.D. degree from the University of Toronto, Toronto, ON, Canada, in 1985, 1988, and 2001, respectively, all in electrical engineering.

From 2001 to 2015, he was with the University of Michigan, Dearborn, MI, USA. He is currently a Professor and the Chair of Electrical and Computer Engineering and the Director with the Department of Energy funded Graduate Automotive Technology Education Center for Electric Drive Transportation, San Diego State University, San Diego, CA, USA.